nature electronics

ARTICLES

https://doi.org/10.1038/s41928-021-00592-y

Check for updates

Body-coupled power transmission and energy harvesting

Jiamin Li[1,4], Yilong Dong[1,4], Jeong Hoan Park[1,2] and Jerald Yoo[1,3]✉

Wireless power transmission and energy harvesting techniques could be used to power and operate devices in, on and around the human body. However, near-field power transmission approaches are limited by distance, and the efficiency of far-field radiofrequency methods is limited by the body shadowing effect. Here, we show that the body-coupling characteristics of electromagnetic waves—which are either artificially introduced or present in the immediate surroundings—can be used to enable a power transmission and energy harvesting method that offers power to locations all around the body. The body-coupled power transmission exhibits a path loss 30- to 70-dB lower than far-field radiofrequency transmission in the presence of body shadowing. The system can recover 2 μW at the head from an ~1.2-mW transmitter placed 160 cm away at the ankle. In the absence of an active power transmitter, we demonstrate placement-independent scavenging of ambient electromagnetic waves coupled onto the human body, resulting in a power recovery of ~2.2 μW from electromagnetic waves of up to −10-dBm on the body.

Wearable sensing networks could be of use in a range of applications, including fitness tracking, health monitoring, remote diagnostics, assisted living, gaming accessories and smart fabrics[1–5]. The wearable devices used to build such networks are heterogeneous and generally need to be placed on specific body locations to deliver the intended functionality. However, providing a stable and sustainable power supply to devices all around the human body remains a challenge[5–10]. Despite recent advances in battery energy density, commercial batteries with a small form factor and reasonable cost still require frequent replacement or recharging. This disrupts network operation and results in inconvenience to users, in particular as the number of electronic nodes in a wearable body area network increases[11–15].

To extend the battery lifetime or sustain fully autonomous operation, power transmission and energy harvesting approaches are required[11,16–34]. Direct wiring to a power source (artificially introduced or ambient harvested) constrains physical movement, and textile-based links (for conduction or waveguides) require special clothing and limit the coverage to textile regions[25]. Approaches based on wireless power transmission, which rely on either inductive coupling[19] or far-field electromagnetic (EM) waves[27,35], are unable to provide efficient power transmission (with >0.01% end-to-end efficiency) to all body locations. For example, inductive coupling typically requires alignment and operates over a short distance, while far-field EM transmission suffers from performance degradation in the body area due to the body shadowing effect, especially in the gigahertz range[27,35,36], with further degradation caused by antenna pattern distortion when in the vicinity of the body[27,36,37] (Supplementary Fig. 1).

Energy harvesting approaches, meanwhile, are often constrained to placement at specific body locations. Photovoltaic-based harvesting requires light exposure, and piezo- and triboelectric nanogenerators that operate via contact electrification need to be placed in areas with physical movement[32,38]. Therefore, devices underneath clothing or with little movement-induced electrostatics (such as an electrocardiogram patch on the chest, earbuds or hearing aid) could not be powered from such sources. The scavenging of EM waves in the air again suffers from the body shadowing effect and is thus dependent on body positioning with respect to the source[27,34].

The human body couples an electric field onto the skin surface, avoiding the body shadowing effect[5,36,39,40]. Indeed, with active circuitry for signal amplification and voltage recovery, the human body has long been utilized as a communication channel[26,41,42]. Some work has attempted to transmit power via body coupling, but this was limited by the voltage gain and thus to a transmission/power recovery distance of <20 cm on a human limb[24,26]. Despite the presence of ambient EM waves—from radio signals, the electrical power grid, electronics and utilities[43]—the harvesting of ambient EM waves via human body coupling remains unexplored. Previous work has focused on EM scavenging in the megahertz to gigahertz range, in air, with an antenna[34]. However, similar to radiofrequency (RF) power transmission, this is subject to the body shadowing effect[27] and is thus affected by the body position with respect to the source.

In this Article, we report a power transmission and ambient energy harvesting method that relies on human body coupling of EM waves (Fig. 1). The approach is based on the complementary metal–oxide–semiconductor (CMOS) chip that we previously optimized for such applications[44,45]. We have developed a transmitter (TX) and receiver (RX)/harvester system using commercially available components that can achieve extended coverage over the entire human body, in an operating frequency range of tens of megahertz. In the absence of an artificially introduced electric field, the system can harvest ambient EM energy, regardless of body area location. Given the commercial availability of most of the components in our system, the approach could be integrated into wearable devices immediately. With our system, we demonstrate wireless and simultaneous powering of multiple digital calculators placed on random human body locations (non-line-of-sight) using transmitted power or power harvested from ambient EM waves.

[1]Department of Electrical and Computer Engineering, National University of Singapore, Singapore, Singapore. [2]Samsung Electronics, Hwaseong, South Korea. [3]The N.1 Institute for Health, National University of Singapore, Singapore, Singapore. [4]These authors contributed equally: Jiamin Li, Yilong Dong. ✉e-mail: jyoo@nus.edu.sg

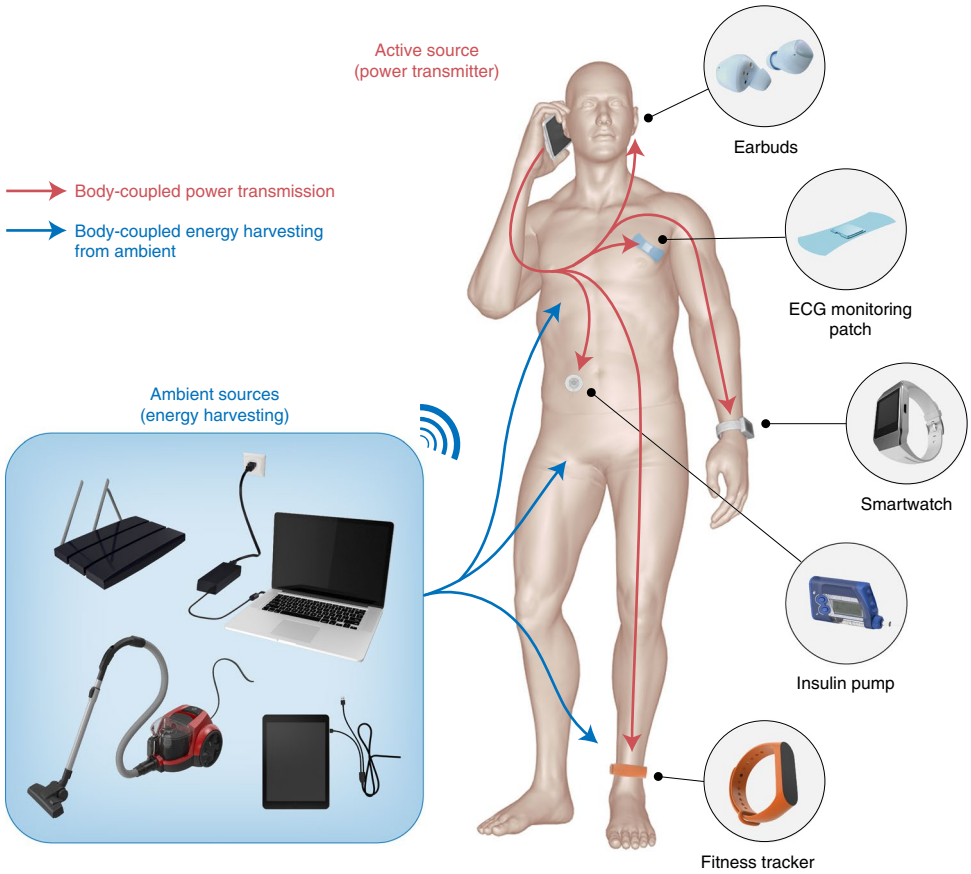

Fig. 1 | The body-coupled power transmission and ambient energy harvesting method. An illustration of the concept, including potential energy sources, potential applications and the power transmission/energy harvesting medium/channel. Red arrows show examples of the power transmission paths across the human body. Blue arrows show the ambient EM waves coupled onto the human body. The power transmitter (active source) and receiver/harvester placements are shown at a few possible locations for illustration purposes.

The human body as power transmission and harvesting medium

In the vicinity of a human body, the channel gain of RF transmission is observed to differ from that in space, especially when the antenna operating wavelength approaches the size of the body (Supplementary Fig. 1; semi-anechoic chamber). A larger antenna operating at lower frequencies (especially below 100 MHz) experiences better channel gain when in contact with the body, with the human body serving as an antenna to facilitate power transmission. However, this requires an antenna with length of about a metre (given the wavelength of ~4–10 m), which is impractical in wearable applications, where miniaturization is essential. Moreover, the channel gain of the RF transmission from the front to the back of the body is approximately −40 dB at the optimal operating frequency, which is still 20 dB lower than the body-coupling mechanism with a wet electrode (Red Dot Ag/AgCl 2237 electrode, 3M; Supplementary Fig. 2). When the antenna length is reduced to 2.9 cm to suit wearable applications (ANT-24G-S21-SMA antenna, RF Solutions), the RF transmission operates at 2.4 GHz and exhibits ~60 dB lower channel gain than the body-coupling method when each is at its optimal operating frequency (Supplementary Fig. 2; semi-anechoic chamber).

Human body-coupled power transmission is found to manifest in the megahertz frequency range, regardless of the transmission path and type of electrode (Supplementary Fig. 3). Although the absolute amount of path loss is dependent on the individual, distance, delivery path and environmental factors, the frequency range of 30–90 MHz exhibits the lowest path loss and was thus chosen as the optimal frequency range for body-coupled power transmission (Supplementary Fig. 4a–c). Unlike RF power transmission, where the antenna size is inversely proportional to the transmission frequency, body coupling is not affected by electrode size and is thus suitable for low-frequency power transmission with a miniaturized transmitter/receiver pair (Supplementary Fig. 4d). Earth ground decoupling was performed and verified (Supplementary Fig. 4e,f). The potential over-the-air direct coupling between cables and electrodes contributed to ~2 to 4 orders of magnitude lower channel gain than the body coupling, and was taken into account (Supplementary Fig. 5). Compared to the conventional far-field RF power transmission method, which is degraded by body shadowing effects[5,36,46], body coupling is mainly affected by the on-body transmission distance and is less susceptible to the transmission paths (Supplementary Fig. 6). The power received by the body coupling (using the 3M Red Dot Ag/AgCl 2237 wet electrode) is 30–70 dB higher compared to RF transmission at 2.4 GHz on and around the body, and up to 50 dB higher compared to RF transmission at 900 MHz (Fig. 2a).

Human body models using an equivalent circuit or a finite element method were proposed for the body-coupled signal communication[47]. We developed a simplified circuit model for the megahertz range, with parasitic capacitances taken into account. Parasitic capacitances are the main contributors to body-coupled power transmission and these could be manipulated during the design process to enhance the power efficiency (Supplementary

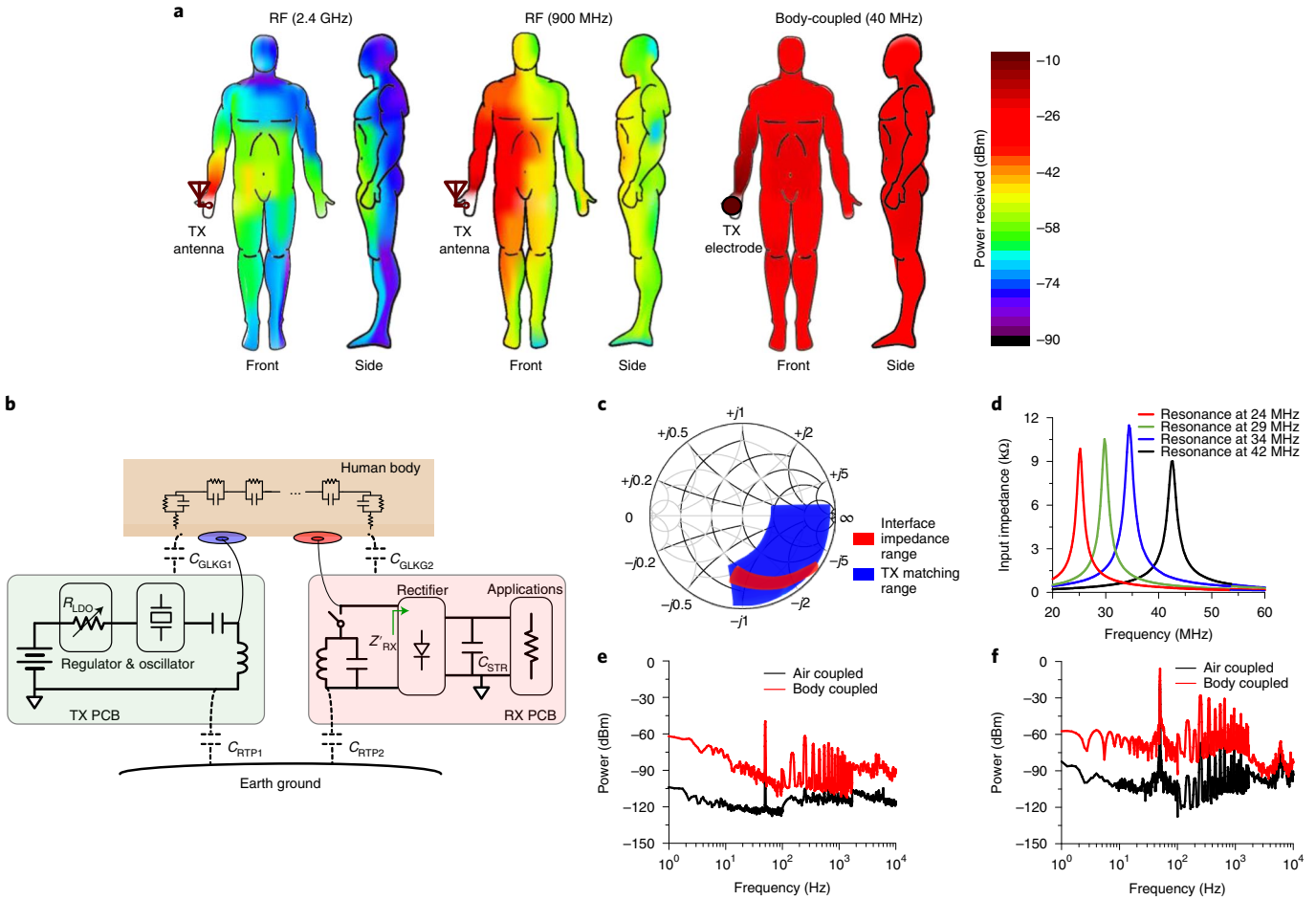

Fig. 2 | Characteristics of the human body as the power-transmission and ambient EM-energy-harvesting medium. a, With a transmitter placed at one hand (emitting 0 dBm), the path gain was measured throughout the body surface. Purple represents the smallest path gain (the largest path loss) and red the highest path gain (the smallest path loss). Front and side views are shown. Horizontally along the body surface, measurements were taken at intervals of 5 cm. Vertically across the body surface, the measurement interval was 5 cm on the head, 10 cm on the arms and 15 cm for on the torso and legs. Averaging was used for interpolation. For the figures on the left, power transmission was implemented by an antenna emitting 0 dBm at 2.4 GHz. For the figures in the middle, power transmission was implemented by an antenna with frequency of 900 MHz emitting 0 dBm. For the figures on the right, power was transmitted via the human body (as the medium), with an electrode as the interface (the transmitter emitted 0 dBm at 40 MHz). The body shadowing of far-field RF power transmission is demonstrated by the degraded path loss under non-line-of-sight condition (left; middle). The same applies when attempting to harvest from ambient RF energy sources. **b**, Schematic of the transmitter and receiver/harvester apparatus and equivalent circuit model of the human body and environmental parasitics. The *LC* impedance booster is a shunt across the receiver front end under the power transmission scheme and is disconnected from the circuitry under ambient energy harvesting. **c**, Smith chart illustrating the impedance matching at the transmitter–skin interface at 50 MHz. The red region represents measured environmental impedance variations mainly contributed by the skin–electrode impedance and return-path parasitic capacitance, whereas the blue region represents the calculated tolerance of the matching scheme in this work. **d**, Measured power receiver input impedance enhanced by the *LC* impedance-boosting circuitry at 24, 29, 34 and 42 MHz, respectively. Deliberate detuning was implemented for each curve. **e**,**f**, Power spectra of ambient EM waves coupled by the human body and air inside a Faraday cage (**e**) and inside an office environment (**f**). The red curve shows the power level measured on the surface of the human body. The black curve shows the power picked up in free space. Both measurements were sensed by an electrode.

Fig. 7). The EM field in the megahertz range was generated by an oscillator powered by a regulated supply voltage (Fig. 2b) and was coupled onto the human body surface via an electrode. The ground node of the transmitter was floated, forming a parasitic capacitance C_{RTP1} with the earth ground for return-path completion. Viewing the transmitter circuit and its environmental interface (including both the electrode and the ground plane interface) as a two-port network, variations of the interface capacitance and resistance of ~0.5–2 pF and ~600–1,000 Ω were observed, with the <1-pF return-path parasitic capacitance being the dominant factor and the electrode impedance the secondary factor (Fig. 2c, red). An L-shaped matching circuit was thus deliberately detuned for wider tolerance (Supplementary Fig. 7b and Fig. 2c, blue) to perform impedance matching with the varying environmental parasitics, improving the reflection coefficient by up to four times (Supplementary Fig. 7c).

At the receiver side, the electrode at the input picks up the EM field and recovers the d.c. power via rectification circuitry (Fig. 2b). The d.c. power is then accumulated at the storage capacitor C_{STR} to provide power to wearable applications. The return path is formed by the parasitic capacitance between the receiver/harvester ground node and the earth ground. With the return-path parasitic capacitance (<1 pF) being the major impedance in the loop, an inductor was added to resonate with the equivalent capacitance of both the extrinsic capacitance C_{EXT} and the receiver intrinsic front-end

capacitance C_{RX} (Fig. 2b and Supplementary Fig. 7d,e). Such an *LC* tank (*L*, inductance; *C*, capacitance) not only boosts the receiver input impedance Z'_{RX} and decouples it from the rectifier input impedance—it is also designed to be in the same impedance range as the return-path capacitance in its resonance frequency (Fig. 2d), allowing improved voltage and power at Z'_{RX} (Supplementary Fig. 7e). Detuning was also performed to reduce its susceptibility to individual, environment, movement and delivery path variations.

A higher parasitic return-path capacitance increases the voltage and power received at the receiver (Supplementary Fig. 7f). Manipulations such as increasing the ground plane size and placing the two ground planes (of transmitter and receiver) near each other contribute to a higher return-path capacitance. However, in practice, with the transmitter and receiver ground planes having the same size as the printed circuit board (PCB; transmitter, 4 cm^2; receiver, 8 cm^2) and being kept at least 10 cm apart from each other and away from any reflective metal surface, the return-path capacitance is generally smaller than 1 pF (ref. [48]). Below 1 pF, the capacitance variations have a negligible influence on the power and voltage received (Supplementary Fig. 7f), thus making further ground plane enlargement unnecessary. By contrast, the capacitive coupling between the elements in the main conduction path (for example, wires, electrodes and the body) and the ground planes of both the transmitter and receiver contributes to the leakage to the earth ground. Stronger coupling and higher capacitance lead to increased leakage and thus lower voltage/power received (Supplementary Fig. 7g). In the design, any direct contact of the ground planes with the human body is avoided to reduce the leakage capacitance.

With the impedance matching and boosting techniques, up to 13 times more power is recovered at the receiver, and the body area coverage is enhanced to the entire arm length (120 cm; Supplementary Fig. 8). The use of impedance matching and boosting enjoys three main benefits. First, a higher voltage can be observed at the receiver or harvester input due to voltage division, which also enhances the power and energy available to the receiver or harvester when designed in the same impedance region as the return-path parasitic capacitance. Second, as the voltage across the rectifier increases, the rectification efficiency increases correspondingly, leading to an overall boost in the end-to-end efficiency. Third, the detuned matching allows for wider impedance tolerance, mitigating the influence of the varying interface or environmental impedance.

Diodes of lower threshold and lower junction capacitance exhibit higher power recovery (Supplementary Fig. 9). The lower threshold allows for higher forward conduction current, whereas the lower junction capacitance leads to increased input impedance (and *Q* in the presence of the *LC* boosting) and also lower leakage at higher frequencies. The load impedance for maximum power extraction varies with different receiver designs. For this receiver apparatus composed of commercially available components (with impedance boosting), the maximum power extraction was observed at a load impedance of 10 kΩ (Supplementary Fig. 10a–c).

For the body-coupling mechanism to be used for ambient energy harvesting, we must first demonstrate the availability of ambient EM waves coupling onto the human body in a normal daily environment. Around 30–40 dB more power was observed when measured on the human body using an electrode (Fig. 2e,f, red) than when measured directly in the air without the human body involved (Fig. 2e,f, black). Compared to measurements performed in a Faraday cage (Fig. 2e), up to 40 dB higher power was coupled onto the body surface in an office (Fig. 2f) and up to 20 dB higher power in a cafeteria (Supplementary Fig. 11). Although waves over a wide spectrum couple onto the human body, waves at 50/60 Hz (due to power line coupling) dominate the spectrum because of the wide usage and ubiquity of the electricity network and appliances. We observe that human body-coupled energy harvesting of EM waves is possible, especially at low frequencies (such as 50/60 Hz), where the conventional use of an antenna for EM energy harvesting would require an antenna size of hundreds of kilometres. The maximum power extraction for ambient energy is observed to occur at a load impedance of 30 MΩ (Supplementary Fig. 10d). With a nano-ampere-range a.c. current induced across the rectifier input and with one floating input node, the leakage contributed by the diode reverse current must be minimized for better power recovery (Supplementary Fig. 12).

Human body-coupled power transmission and energy harvesting

The transmitter and receiver/harvester were fabricated on a PCB with commercially available components (Fig. 3a) and occupied areas of 2 × 2 cm^2 (transmitter) and 2 × 4 cm^2 (receiver). Wet electrodes (Red Dot Ag/AgCl 2237, 3M) were used to pick up the electric field on the body surface and relay it to the receiver input. The transmitter was sustained by battery power, but the receiver/harvester operated solely using the recovered power.

The recovered power correlates positively with transmission power (Fig. 3b) and negatively with increasing transmission distance (Fig. 3c, left). With the transmitter and receiver 15 cm apart, 0.8 mW of power was recovered by the apparatus when the power transmitter output was 13.5 mW and 10 V_{PP}. At the same distance, with a reduced transmitter output of 3 V_{PP} and ~1.2 mW, 53 μW was recovered (Fig. 3b). With increased distance, with the power transmitter (placed at one wrist) emitting ~1.2 mW at 3 V_{PP}, 1.1 μW was recovered at the other wrist. This distance was estimated to be 120 cm considering the length of an adult arm (male, height 170 cm). When the transmitter was placed at an ankle and the receiver at the forehead (an equivalent on-body transmission distance of 160 cm), 2 μW was recovered (with 3 V_{PP} transmitter output) (Fig. 3c, left). The higher recovered power compared to the wrist case is attributed to the higher capacitive coupling with the earth ground when one node is placed at the ankle. Compared with previous attempts at using the human body for power transmission[24,26], which required a close distance between the transmitter and receiver (less than 20 cm, equivalently), our apparatus shows eight times improvement in body area coverage (Fig. 3c). Far-field RF power transmission, in contrast, experiences a path loss greater than 40 dB when the transmission distance increases to over ~15 cm at 2.4 GHz and over ~60 cm at 900 MHz (Fig. 2a, left and Supplementary Fig. 6). As this is equivalent to less than 100 nW recoverable from 1 mW transmitted, we consider it to have fallen out of effective coverage, resulting in a coverage range 10.7 times and 2.7 times smaller than that of our method (Fig. 3c, right).

We also observed that the recovered power and open-circuit voltage were not affected by the number of other nodes (up to 10) concurrently extracting power introduced by the body coupling (Fig. 3d) when the transmitter power was ~1.2 mW. There will be a limit where a further increase in the number of concurrent receiving nodes will degrade the power recoverable at each node, but this is not of practical concern, as the use case of more than 10 wearables operating concurrently will be rare, and this limit could be overcome by increasing the transmitter power. This characteristic suggests the feasibility of simultaneous one-to-many power transmission. Moreover, as the electrode is down- and up-sized, a similar amount of power and open-circuit voltage is recovered (Fig. 3e). Unlike far-field RF power transmission and near-field inductive coupling, where the antenna and coil sizes are determined by the operating frequency, we can potentially further downscale each sensor node size.

The receiving nodes can continuously scavenge body-coupled ambient EM waves (with the *LC* boosting circuit disconnected from the RX front end), which is especially helpful in the absence of an active power-transmitting source. Constrained by the environment dependency inherent in any energy harvesting approach, the

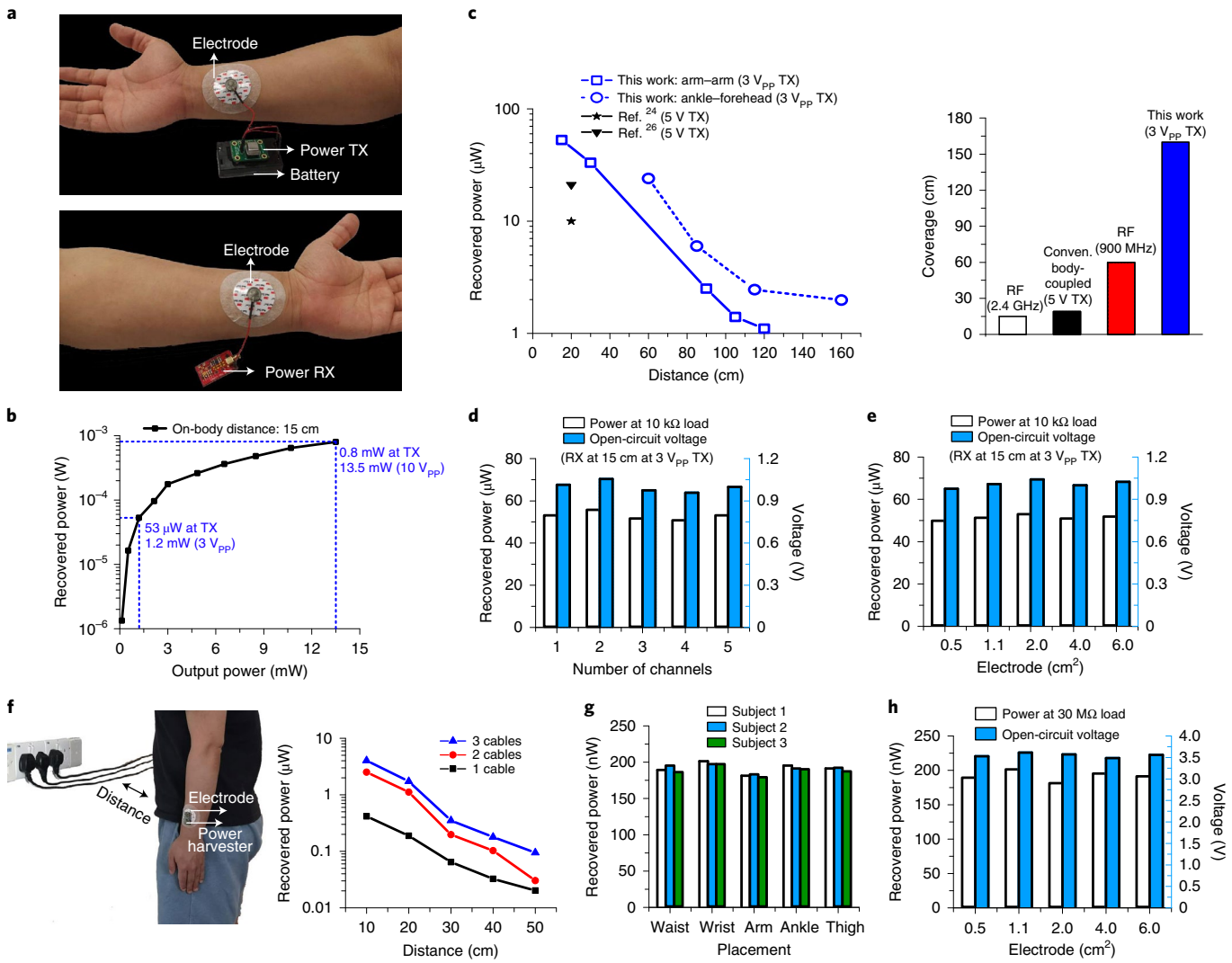

Fig. 3 | The amount and characteristics of power recovered via the human body as medium. a, Photograph of the power transmitter (top) and the receiver/harvester board (bottom, worn on the human wrist). Commercially available wet electrodes (Red Dot Ag/AgCl 2237, 3M) were used for the skin interface. **b**, Correlation between the power recovered and the transmitter output power. **c**, Power recovered (at a load of 10 kΩ) with respect to on-body distance using the method and apparatus in this work, in comparison with previous attempts at using a body channel for power transmission[24,26] (left) and conventional RF power transmission approaches (right). **d**, Recovered power (at a load of 10 kΩ) and open-circuit voltage at a receiving node placed 15 cm away from the transmitter versus the number of simultaneous receiving nodes in the network. The transmitter output is 3 V_{pp} and ~1.2 mW. **e**, Recovered power (at a load of 10 kΩ) and open-circuit voltage versus electrode area of the transmitter and receiver, which were placed 15 cm apart. **f**, Power recovered with respect to the distance from a potential ambient power source. The measurement environment is controlled, with the power cables being the only ambient power source. The cables were open-ended (no electrical devices or equipment connected). **g**, Power recovered with a 30-MΩ load resistor by five harvesters simultaneously placed on different parts of the body, with one electrical power line placed 20 cm away from the body. Power recovered from three individuals is shown. **h**, Power recovered with a 30-MΩ resistor and open-circuit voltage, achieved with various electrode areas. The harvester was placed on the right wrist of subject 1, and measurements were made with one electrical power line placed 20 cm away from the body.

amount of power that can be scavenged by our method is susceptible to the existence of EM waves in the environment. The amount of power lines and access to them, as well as the presence of electrical appliances and charging electronic devices, could all influence the amount harvested. For example, in an office setting where up to −10 dBm is observed (Fig. 2f), ~2.2 µW could be recovered. In an environment where up to −30 dBm is observed (Supplementary Fig. 11), ~100 nW could be recovered. Figure 3f shows the recovered power with respect to body distance from the ambient power source in a controlled environment where the only source is electrical power lines. Although up to ~4 µW could be recovered in the presence of three electrical power lines placed 10 cm apart, this decreased to ~100 nW when the distance was increased to 50 cm. When charging a laptop, up to ~2 µW could be recovered at a distance of 50 cm (Supplementary Fig. 13). In spite of its environmental dependency (an intrinsic characteristic of any harvesting approach), a body-coupled ambient energy harvesting scheme could be used to complement body-coupled power transmission for longer sustainability, with both recovering power via the body channel (either introduced artificially by a dedicated transmitter or naturally from the surroundings).

As a result of individual-based differences in tissue electrical characteristics, the recoverable ambient energy varies from person to person, even if they have the same posture and positioning and the same environment (Fig. 3g). For any particular individual, the amount of recovered power remains similar, regardless of where

Table 1 | Comparison of body-coupled power transmission with conventional body area power transmission techniques, including near-field inductive coupling, far-field RF power transmission and ultrasound power transmission

	Inductive coupling[19]	Far-field power transfer[27]	Ultrasound power transfer[17,31]	Body-coupled power transmission (this work)
Frequency	13.56 MHz	1 GHz	1 MHz	30–90 MHz
Transmitter power	1 mW	15 W	1 mW	~1.2 mW
Distance	<4 cm	1,500-cm line of sight	3 cm	Full body area
Recovered power	5 μW at 4 cm with perfect alignment	30 mW at 1,500-cm line of sight	57 μW at 3 cm	53 μW at 15 cm 2 μW at 160 cm (both at 40 MHz)
Coverage	Short distance; placements with achievable TX and RX alignment	Transmitter location dependent; receiver placements under body shadowing effect are not covered	Mostly implants	Full body; not affected by the body shadowing effect
Operating condition	Coil alignment	No major obstruction in the transmission path; not under body shadowing region	Line of sight	No special condition required

Table 2 | Comparison of body-coupled ambient energy harvesting with conventional body area energy harvesting techniques, including photovoltaics harvesting, thermal energy harvesting, piezoelectric harvesting, triboelectric harvesting and far-field RF energy harvesting

	Photovoltaics harvester[18]	Thermoelectric harvester[21,28]	Piezoelectric harvester[16,20,32]	Triboelectric harvester[22,29]	RF harvester[27,34]	Body-coupled ambient EM harvesting (this work)
Environment controlled	Light exposure 100–100k lux	Heat flow at 22 °C ambient temperature	Vibration frequency > 100 Hz	Friction frequency generation > 1 Hz	20-dBm transmitter at 2.4 GHz ~3 m facing the front of body	Ambient EM waves > −30 dBm
Head (electroencephalogram; hearing aid)	√	√	X	X	√	√
Chest (electrocardiogram)	X	Unless embedded within clothing to ensure heat flow (costly)	X	X	√	√
Waist	X		X	X	√	√
Back	X		X	X	X	√
Thigh	X		X	X	√	√
Wrist	X	√	X	√	√	√
Foot	X	X	√	√	√	√
Average power available in controlled environment	10 μW cm^{-2}–10 mW cm^{-2}	20 μW cm^{-2}	30 μW cm^{-2} at 143 Hz	77 nW cm^{-2} at 1 Hz; 1.5–5.3 μW cm^{-2} at 50 Hz	~−30 dBm	~−30 dBm to −14 dBm

the electrodes are placed, with only slight fluctuations (Fig. 3g). Among the locations investigated were those with little movement- or pressure-induced electrostatics and little daylight coverage due to clothing. Such homogeneity in terms of the amount harvested at different placements indicates the wide potential body area coverage of the proposed ambient energy harvesting method, which would allow devices placed on the chest, such as electrocardiogram sensors, to operate on the recovered power. Moreover, with multiple nodes operating simultaneously, the amount of energy harvested by each node remains similar to that harvested by a single node operating alone, allowing for multi-node energy harvesting without inter-dependency. With a reduction in electrode size, the amount harvested remains similar, despite fluctuations (Fig. 3h), suggesting the irrelevance of electrode size to power recoverability with the proposed method, as well as the potential for device downscaling.

To demonstrate the simultaneous power transmission to wearable nodes across the entire body, as well as simultaneous energy harvesting at various wearable nodes regardless of their locations on the body, a commercial digital calculator (with its battery removed) was connected to and solely powered by the body-coupled powering apparatus (Supplementary Fig. 14). Supplementary Fig. 14a shows that the power recovered simultaneously at each of three different placements is sufficient to power up and sustain the operation of a digital calculator (Supplementary Video 1). Supplementary Fig. 14b shows that, after 3 min of ambient EM energy scavenging through the human body, energy collected at each of the three different placements is sufficient to power up the calculator and sustain a few operations (Supplementary Video 2).

Numerical examples of the average power requirements of wearable applications are summarized in Supplementary Table 1, along with the power-sustaining capability of the proposed body-coupled powering (harvesting and transmission). For low-power wearables consuming up to a microwatt (for example, a temperature sensor, electrocardiogram sensor with arrhythmia detection, blood

pressure monitor, radiation dosimeter, glucose sensor and low-data-rate transmission), both the body-coupled ambient harvesting (with the body-coupled power level ranging from −30 dBm to −10 dBm) and the body-coupled power transmission (with an active power source outputting 1.2 mW) could independently sustain operations around the entire body area, posing no restrictions on where the nodes should be worn. As the power budget increases to tens to hundreds of microwatts (for example, a multi-sensor ExG (physiological signals such as electroencephalogram, electrocardiogram, electromyogram, and so on) system-on-chip or a hearing aid), continuous harvesting from the surroundings could complement the power available at the node, although it might not suffice when used alone. A higher transmitter output power is required (for example, 13.5 mW) for an extended on-body transmission distance. For applications such as a high-data-rate (for example, Mbps) transceiver, electrical impedance tomography or inertial navigation systems, which require a power budget of >1 mW, on-board processing for data rate reduction or duty cycling (allowed by the slow physical dynamics monitored) should be performed for the body-coupled powering to function as a sole power source.

Unlike conventional body area power transmission[17,19,27,31] and energy harvesting approaches for wearable nodes[16,18,20–22,27–29,32,34], the body-coupled power transmission and ambient energy harvesting method and apparatus in this work both support coverage of the entire human body (Table 1). Thanks to the low path loss inherent in this power transmission method and the circuit techniques employed, higher end-to-end power recovery could be achieved. Moreover, unlike conventional harvesters, which have specific placement requirements to meet, this energy harvesting method is applicable across the human body regardless of clothing coverage or body blockage (Table 2).

The proposed body-coupled power transmission scheme is strictly below the specific absorption rate (SAR) limit for the whole body and local body parts. Considering a power transmitter introducing an electric field with an output power of ~1.2 mW at ~20–100 MHz, the whole-body SAR is calculated to be 2×10^{-5} W kg^{-1}, using

$$\text{Whole body SAR} \leq 1.2\,\text{mW}/60\,\text{kg} = 2\times10^{-5}\,\text{W kg}^{-1}$$

for an average body weight of 60 kg. With an enhancement in transmitter voltage to 10 V_{PP} (~13.5 mW output power; Fig. 3c), the whole-body SAR is calculated to be 2.5×10^{-4} W kg^{-1}. Both values are four orders of magnitude below the Federal Communications Commission limit of 1.6 W kg^{-1}. For the power transmission system model (Supplementary Fig. 7), the electric field across the body is shown in Supplementary Fig. 15 with respect to variations in the return-path capacitance $C_{RTP1,2}$ and leakage capacitance $C_{GLKG1,2}$. At below 0.039 V m^{-1} under 1.2-mW transmitter output and below 0.128 V m^{-1} under 13.5-mW transmitter output, the electric field developed is lower than the IEEE threshold of 2.1 V m^{-1} under a controlled environment and 0.701 V m^{-1} for the general public[49]. Moreover, other than the a.c. signals coupled on the body, there is no d.c. current flow through the human body in either case, as the return path is formed by the capacitive coupling between one node of the rectifier input and the earth ground.

Conclusions

We have reported a body-coupled power transmission and ambient EM energy harvesting system that can be used to provide sustainable power for wearable devices all around the human body. By exploiting the body-coupling characteristics of both an actively introduced electric field and ambient EM waves, this approach can avoid the body shadowing effect. We have demonstrated the coverage and effectiveness of the method with a transmitter and receiver/harvester apparatus with impedance matching and boosting techniques. A power of 52 μW could be recovered at 15 cm and 2 μW at 160 cm away from a transmitter outputting ~1.2 mW at 3 V_{PP}. At 15 cm apart and when the transmitter output voltage increases to 10 V_{PP}, 0.8 mW could be recovered. A power of 2.2 μW could be harvested from an ambient body-coupled EM energy of up to −10 dBm, independent of electrode placement and size. Our approach overcomes the challenges of limited on-body power transmission distance and placement-dependent energy harvesting and could be used to develop miniaturized wearable devices with enhanced power recovery and scavenging efficiency and reliability for use across the entire body.

Methods

Transmitter and receiver/harvester prototype design. The transmitter, fabricated on a PCB (thickness of 1.5 mm, Au electroplating pad), consists of a battery pack (3/6 V), a regulator (Microchip, MCP1700T-3302E/TT), crystal oscillators (ALE Crystals) with standard high-speed CMOS (HCMOS) or transistor–transistor logic (TTL) output, and matching circuitry (Coil Craft 1008CS series inductor and AVX RF capacitor with 0603 package) at its output. This couples power via a wet electrode (Red Dot Ag/AgCl 2237, 3M) onto the human body. The harvester/receiver receives the signal via the wet electrode and passes it to rectification circuitry (thickness of 1.5 mm, Au electroplating pad). The receiver rectifier is shunted by an *LC* tank (Coil Craft 1008CS series inductor and AVX RF capacitor with 0603 package) at the input and is itself built as a bridge configuration of four RF Schottky diodes (Skyworks, SMS7621-060) with one input node floating. The harvester rectifier is built as the bridge configuration of four RF PIN diodes (Infineon, BAR6303WE6327HTSA1). A commercial surface mount device (SMD)-type capacitor and resistor are used for storage and loading.

Path loss characterization of the body-coupled power transmission. Two wet electrodes (Red Dot Ag/AgCl 2237, 3M) are attached on the skin, one for electric field coupling from the power transmitter onto the body surface, and the other for use at the receiving node for power recovery. A RF vector signal generator (Keysight, EXG Vector Signal Generator, N5172B) serves as the source for active power delivery in this measurement. The RF generator delivers 6.8 dBm of power under a 50-Ω matched load impedance. It is not practical to meet the condition of a matched impedance for body channel measurements due to variations in the transmitter–skin interface impedance caused by the skin–electrode contact, environmental and individual induced parasitic changes. Therefore, the path loss of the body channel is still measured in this way to give a relative indication of the channel performance, whereas the actual end-to-end efficiency is measured with the actual transmitter output and the recovered d.c. power at the receiver. Supplementary Fig. 7c shows the transmitter reflection coefficient measured over the target operating frequency in the megahertz range. The single-ended signal coming out of the RF generator is first converted to the differential by a balun (Mini-Circuits, Transformer, FTB-1-6*A15+), then one node is connected to the electrode and the other is cut off and left floating. This is to simulate the actual scenario where a receiving node is worn on the body and the return path is formed by capacitive coupling with the earth ground, rather than an explicit connection. At the receiving end, the alternating field coupled across the rectifier input (with one node floating) first passes through a balun (Mini-Circuits, Transformer, FTB-1-6*A15+) for differential to single-ended conversion, and is then fed into the RF spectrum analyser (Keysight, EXA Signal Analyser, N9010A, 10 Hz–3.6 GHz) for power measurement. The resolution bandwidth of the RF spectrum analyser was set to 1 kHz. The set-up configuration is illustrated in Supplementary Fig. 16a.

To eliminate the influence of cable-induced power loss, as well as potential coupling between electrode cables in the measurement of body path loss, the power received across the rectifier input due to coupling alone and the path loss due to cables are measured each time there is a change in cable configuration, then decoupled from the measurement results of body path loss (Supplementary Fig. 5).

These techniques effectively decouple the potential earth ground connection of the energy transmitter and receiver, thereby creating a testing environment similar to the actual scenario where a battery-operated transmitter emits power to sustain receiving nodes. This was further verified by measuring and comparing the received power at the rectifier input, with the power transmitter being the battery-powered PCB (Supplementary Fig. 16b). As illustrated in Supplementary Fig. 4e,f, similar trends and power levels could be observed, indicating that the RF generator and spectrum analyser (Keysight, EXA Signal Analyser N9010A, 10 Hz–3.6 GHz) are properly decoupled and could be utilized to emulate an actual usage scenario (with battery-operated devices).

Measurements of human body coupling of ambient EM waves. A wet electrode (Red Dot Ag/AgCl 2237, 3M) was attached onto the skin and connected to the dynamic signal analyser (Keysight, 35670A) input. The ground of the dynamic signal analyser was separated from the earth ground by the uninterrupted power supply (Scott Power) to ensure the capacitively coupled return path and emulate the actual environmental characteristics experienced by the harvester. The uninterrupted power supply (Scott Power) was powered by its battery backup, which

then performed the d.c. to a.c. conversion for the dynamic signal analyser (Keysight, 35670A) supply. The configuration is illustrated in Supplementary Fig. 16c.

Path loss characterization of antenna-based RF power transmission in the body vicinity. The transmitting antenna (ANT-24G-S21-SMA, manufactured by RF solutions for the 2.4-GHz measurement, or SPDA24918, manufactured by PulseLarsen Antennas for the 900-MHz measurement; both matched at 50 Ω) was placed on one hand of the subject. The RF vector signal generator (Keysight, EXG Vector Signal Generator, N5172B) was connected with the antenna and served as the power source with 0-dBm output power. The path loss throughout the human body was measured by a receiving antenna connected with a spectrum analyser (Keysight, EXA Signal Analyser N9010A, 10 Hz–3.6 GHz, 50-Ω input matching impedance). The measurements were conducted in a semi-anechoic chamber (electric field attenuation of >100 dB from 10 kHz to 40 GHz), as illustrated in Supplementary Fig. 17.

Comparison measurements of the body channel behaviour using the body-coupling approach with the wet electrode (Red Dot Ag/AgCl 2237, 3M)/dry electrode (2-cm^2 copper sheet) were also conducted in the same semi-anechoic chamber, with a similar set-up, as illustrated in Supplementary Fig. 18.

Power recovery via body-coupled power transmission. Two wet electrodes (Red Dot Ag/AgCl 2237, 3M) were attached on the skin, and the transmitter PCB (described earlier) was used to couple the electric field onto the human body. The transmitter output was ~1.2 mW with 3 V_{PP}. The receiver incorporated rectification circuitry with an *LC* tank shunted across the rectifier input for both power and voltage boosting. The resonance frequency was the same as the energy delivery frequency, and the inductor and capacitor values were selected based on the *LC* resonance equation $f = \sqrt{1/4\pi^2 LC}$, as well as *Q*-factor (quality factor) considerations. A load capacitor of 10 nF was shunted across the rectifier output for energy storage. An oscilloscope (Keysight, DSOX3034T with a sampling rate of 5 Gsamples s^{-1}) was then used for output voltage measurements, from which the rectified d.c. power was calculated by $P = V^2/R_{load}$. Two oscilloscope probes (Keysight, N2843A, 10:1) for channel 1 and channel 2 inputs were used to probe at the two nodes of the rectifier output, respectively, with both group leads connected together and left floating. The voltage difference between these two channels was taken as the output voltage to counteract potential fluctuations due to ambient noise. The configuration of the set-up is illustrated in Supplementary Fig. 19a.

The open-circuit voltage was measured with an oscilloscope (Keysight DSOX3034T, with a sampling rate 5 Gsamples s^{-1}) by removing all resistive components from the rectifier load at the receiver side, and shunting the oscilloscope probe (Keysight N2843A, 10:1) across the load capacitor (impedance, 10 MΩ).

Energy scavenging via body-coupled ambient energy harvesting. A wet electrode (Red Dot Ag/AgCl 2237, 3M) was attached to the skin to transfer the charges coupled on the body onto one input node of the harvester. A portable picoscope (Pico Technology, 4424) was used for output voltage measurements, from which the rectified d.c. power was calculated by $P = V^2_{store}/R_{load}$. A picoscope probe (Pico Technology, 10:1) was used to probe at the rectifier output to determine V_{store}. An analogue buffer (Analog Devices, AD8065) with a common-mode impedance of 1,000 GΩ at 2.1 pF was inserted between the resistive load and the picoscope probes to eliminate the loading effect caused by the 10-MΩ probes. The set-up configuration is illustrated in Supplementary Fig. 19b.

Reporting Summary. Further information on research design is available in the Nature Research Reporting Summary linked to this Article.

Data availability

The data that support the plots within this paper and other findings of this study are available from the corresponding author upon reasonable request.

Received: 9 March 2020; Accepted: 30 April 2021;
Published online: 10 June 2021

References

1. Gao, W. et al. Fully integrated wearable sensor arrays for multiplexed in situ perspiration analysis. *Nature* **529**, 509–514 (2016).
2. Son, D. et al. Multifunctional wearable devices for diagnosis and therapy of movement disorders. *Nat. Nanotechnol.* **9**, 397–404 (2014).
3. Daniels, J. et al. Exploratory study examining the at-home feasibility of a wearable tool for social-affective learning in children with autism. *npj Digital Med.* **1**, 32 (2018).
4. Negra, R., Jemili, I. & Belghith, A. Wireless body area networks: applications and technologies. *Proc. Comput. Sci.* **83**, 1274–1281 (2016).
5. Yoo, J. & Yoo, H.-J. in *Bio-Medical CMOS ICs* (eds Yoo, H.-J. & van Hoof, C.) 339–370 (Springer, 2011).
6. Yamamoto, Y. et al. Printed multifunctional flexible device with an integrated motion sensor for health care monitoring. *Sci. Adv.* **2**, e1601473 (2016).
7. Lee, H. et al. Toward all-day wearable health monitoring: an ultralow-power, reflective organic pulse oximetry sensing patch. *Sci. Adv.* **4**, eaas9530 (2018).
8. Zeng, W. et al. Fiber-based wearable electronics: a review of materials, fabrication, devices and applications. *Adv. Mater.* **26**, 5310–5336 (2014).
9. Bandodkar, A. J., Jeerapan, I. & Wang, J. Wearable chemical sensors: present challenges and future prospects. *ACS Sens.* **1**, 464–482 (2016).
10. Patel, S., Park, H., Bonato, P., Chan, L. & Rodgers, M. A review of wearable sensors and systems with application in rehabilitation. *J. Neuroeng. Rehabil.* **9**, 21 (2012).
11. Wang, J. et al. Sustainably powering wearable electronics solely by biomechanical energy. *Nat. Commun.* **7**, 12744 (2016).
12. Peng, M. et al. Efficient fiber shaped zinc bromide batteries and dye sensitized solar cells for flexible power sources. *J. Mater. Chem. C* **3**, 2157–2165 (2015).
13. Park, J., Park, M., Nam, G., Lee, J.-S. & Cho, J. Zinc-air batteries: all-solid-state cable-type flexible zinc-air battery. *Adv. Mater.* **27**, 1395–1395 (2015).
14. Gaikwad, A. M., Whiting, G. L., Steingart, D. A. & Arias, A. C. Highly flexible, printed alkaline batteries based on mesh-embedded electrodes. *Adv. Mater.* **23**, 3251–3255 (2011).
15. Dong, K. et al. A highly stretchable and washable all-yarn-based self-charging knitting power textile composed of fiber triboelectric nanogenerators and supercapacitors. *ACS Nano* **11**, 9490–9499 (2017).
16. Zhao, J. & You, Z. A shoe-embedded piezoelectric energy harvester for wearable sensors. *Sensors* **14**, 12497–12510 (2014).
17. Link, B. D., Charthad, J., Member, S., Weber, M. J. & Member, S. A mm-sized implantable medical device (IMD) with ultrasonic power transfer and a hybrid bi-directional data link. *IEEE J. Solid State Circuits* **50**, 1741–1753 (2015).
18. Chen, P. H., Wu, C. S. & Lin, K. C. A 50 nW-to-10 mW output power tri-mode digital buck converter with self-tracking zero current detection for photovoltaic energy harvesting. *IEEE J. Solid State Circuits* **51**, 523–532 (2016).
19. Abiri, P. et al. Inductively powered wireless pacing via a miniature pacemaker and remote stimulation control system. *Sci. Rep.* **7**, 6180 (2017).
20. Kwon, D. & Rincon-Mora, G. A. A single-inductor 0.35-μm CMOS energy-investing piezoelectric harvester. *IEEE J. Solid State Circuits* **49**, 2277–2291 (2014).
21. Leonov, V., Torfs, T., Fiorini, P. & Van Hoof, C. Thermoelectric converters of human warmth for self-powered wireless sensor nodes. *IEEE Sens. J.* **7**, 650–657 (2007).
22. Park, I. et al. A 4.5-to-16 μW integrated triboelectric energy-harvesting system based on high-voltage dual-input buck converter with MPPT and 70-V maximum input voltage. In *Proc. IEEE International Solid-State Circuits Conference* (*ISSCC*) *Digest of Technical Papers* (ed. Fujino, L. C.) Vol. 61, 146–148 (IEEE, 2018).
23. Kim, T. et al. Flexible, highly efficient all-polymer solar cells. *Nat. Commun.* **6**, 8547 (2015).
24. Wang, E. J., Sharma, M., Zhao, Y. & Patel, S. N. CASPER: capacitive serendipitous power transfer for through-body charging of multiple wearable devices. In *Proc. 2018 ACM International Symposium on Wearable Computers* 188–195 (ACM, 2018).
25. Tian, X. et al. Wireless body sensor networks based on metamaterial textiles. *Nat. Electron.* **2**, 243–251 (2019).
26. Cho, H. et al. An area-efficient rectifier with threshold voltage cancellation for intra-body power transfer. In *Proc. IEEE International Symposium on Circuits and Systems* (*ISCAS*) 1–5 (IEEE, 2019).
27. Huang, X. et al. Epidermal radio frequency electronics for wireless power transfer. *Microsyst. Nanoeng.* **2**, 16052 (2016).
28. Katic, J., Rodriguez, S. & Rusu, A. A dual-output thermoelectric energy harvesting interface with 86.6% peak efficiency at 30 μW and total control power of 160 nW. *IEEE J. Solid State Circuits* **51**, 1928–1937 (2016).
29. Sano, C. et al. Triboelectric energy harvesting with surface-charge-fixed polymer based on ionic liquid. *Sci. Technol. Adv. Mater.* **19**, 317–323 (2018).
30. Cottrill, A. L. et al. Ultra-high thermal effusivity materials for resonant ambient thermal energy harvesting. *Nat. Commun.* **9**, 664 (2018).
31. Dinis, H., Colmiais, I. & Mendes, P. M. Extending the limits of wireless power transfer to miniaturized implantable electronic devices. *Micromachines* **8**, 12 (2017).
32. Shenck, N. S. & Paradiso, J. A. Energy scavenging with shoe-mounted piezoelectrics. *IEEE Micro* **21**, 30–42 (2001).
33. Gong, S. et al. A wearable and highly sensitive pressure sensor with ultrathin gold nanowires. *Nat. Commun.* **5**, 3132 (2014).
34. Sadagopan, K. R., Kang, J., Ramadass, Y. & Natarajan, A. A 960 pW co-integrated-antenna wireless energy harvester for WiFi backchannel wireless powering. In *Proc. IEEE International Solid-State Circuits Conference* (*ISSCC*) *Digest of Technical Papers* (ed. Fujino, L. C.) Vol. 61, 136–138 (IEEE, 2018).
35. Cotton, S. L., D'Errico, R. & Oestges, C. A review of radio channel models for body centric communications. *Radio Sci.* **49**, 371–388 (2014).

36. Kifle, Y., Kim, H. S. & Yoo, J. Human body and head characteristics as a communication medium for body area network. In *Proc. 2015 Annual International Conference of the IEEE Engineering in Medicine and Biology Society*, *EMBS* 1845–1848 (IEEE, 2015).
37. Cho, H., Bae, J. & Yoo, H. J. A 37.5-μW body channel communication wake-up receiver with injection-locking ring oscillator for wireless body area network. *IEEE Trans. Circuits Syst. I Regul. Pap.* **60**, 1200–1208 (2013).
38. Roundy, S., Wright, P. K. & Rabaey, J. M. *Energy Scavenging for Wireless Sensor Networks: With Special Focus on Vibrations* (Kluwer Academic, 2004).
39. Cho, N. et al. The human body characteristics as a signal transmission medium for intrabody communication. *IEEE Trans. Microw. Theory Tech.* **55**, 1080–1086 (2007).
40. Zimmerman, T. G. Personal area networks: near-field intrabody communication. *IBM Syst. J.* **35**, 609–617 (1996).
41. Bae, J., Cho, H., Song, K., Lee, H. & Yoo, H.-J. The signal transmission mechanism on the surface of human body for body channel communication. *IEEE Trans. Microw. Theory Tech.* **60**, 582–593 (2012).
42. Fort, A. et al. Ultra-wideband channel model for communication around the human body. *IEEE J. Sel. Areas Commun.* **24**, 927–933 (2006).
43. Staebler, P. *Human Exposure to Electromagnetic Fields*: *From Extremely Low Frequency* (*ELF*) *to Radiofrequency* (Wiley, 2017).
44. Li, J. et al. Human-body-coupled power-delivery and ambient-energy-harvesting ICs for a full-body-area power sustainability. In *Proc. IEEE International Solid-State Circuits Conference* (*ISSCC*) *Digest of Technical Papers* (ed. Fujino, L. C.) Vol. 63, 514–515 (IEEE, 2020).
45. Li, J. et al. Body-area powering with human body-coupled power transmission and energy harvesting ICs. *IEEE Trans. Biomed. Circuits Syst.* **14**, 1263–1273 (2020).
46. Yoo, J. Body coupled communication: towards energy-efficient body area network applications. In *Proc. 2017 IEEE International Symposium on Radio-Frequency Integration Technology* (*RFIT*) 244–246 (IEEE, 2017); https://doi.org/10.1109/rfit.2017.8048239
47. Park, J., Garudadri, H. & Mercier, P. P. Channel modeling of miniaturized battery-powered capacitive human body communication systems. *IEEE Trans. Biomed. Circuits Syst.* **64**, 452–462 (2017).
48. Mao, J., Yang, H. & Zhao, B. An investigation on ground electrodes of capacitive coupling human body communication. *IEEE Trans. Biomed. Circuits Syst.* **11**, 910–919 (2017).
49. *IEEE Standard for Safety Levels With Respect to Human Exposure to Radio Frequency Electromagnetic Fields*, *3 kHz to 300 GHz*, IEEE Std C95.1-2005 (revision of IEEE Std C95.1-1991) (IEEE, 2006).

Acknowledgements

We thank A. Thean for helpful discussions, J. Ho and R. J. M. Yap for support with rectifier devices and Y. Kifle for the set-up of the body channel measurements. We acknowledge support from the Semi-anechoic Chamber at Electromagnetic Effects Research Laboratory (EMERL), jointly operated by Nanyang Technological University Singapore and DSO National Laboratories Singapore, and J. M. M. Low for his support at EMERL. This work was funded by the NUS Hybrid-Integrated Flexible Electronic Systems Program (R-263-501-009-731) as well as A*STAR AME Nanosystems at the Edge Program under grant no. A18A4b0055.

Author contributions

J.Y. produced the idea of body-coupled energy harvesting/power transmission, proposed the research direction and supervised the project. J.L. and Y.D. conceived and designed the experiments. J.L. wrote the manuscript and Y.D. produced the figures. J.L., Y.D. and J.H.P. collected and analysed the data. Y.D. designed the harvester and transmitter. All authors discussed and reviewed the manuscript.

Competing interests

The authors declare no competing interests.

Additional information

Supplementary information The online version contains supplementary material available at https://doi.org/10.1038/s41928-021-00592-y.

Correspondence and requests for materials should be addressed to J.Y.

Peer review information *Nature Electronics* thanks Ada Poon, Jan Rabaey and Jeremy Gummeson for their contribution to the peer review of this work.

Reprints and permissions information is available at www.nature.com/reprints.

Publisher's note Springer Nature remains neutral with regard to jurisdictional claims in published maps and institutional affiliations.

nature research

Corresponding author(s): Jerald Yoo

Last updated by author(s): Apr 29, 2021

Reporting Summary

Nature Research wishes to improve the reproducibility of the work that we publish. This form provides structure for consistency and transparency in reporting. For further information on Nature Research policies, see our Editorial Policies and the Editorial Policy Checklist.

Statistics

For all statistical analyses, confirm that the following items are present in the figure legend, table legend, main text, or Methods section.

n/a	Confirmed	
☐	☒	The exact sample size (*n*) for each experimental group/condition, given as a discrete number and unit of measurement
☐	☒	A statement on whether measurements were taken from distinct samples or whether the same sample was measured repeatedly
☒	☐	The statistical test(s) used AND whether they are one- or two-sided *Only common tests should be described solely by name; describe more complex techniques in the Methods section.*
☒	☐	A description of all covariates tested
☒	☐	A description of any assumptions or corrections, such as tests of normality and adjustment for multiple comparisons
☐	☒	A full description of the statistical parameters including central tendency (e.g. means) or other basic estimates (e.g. regression coefficient) AND variation (e.g. standard deviation) or associated estimates of uncertainty (e.g. confidence intervals)
☒	☐	For null hypothesis testing, the test statistic (e.g. *F*, *t*, *r*) with confidence intervals, effect sizes, degrees of freedom and *P* value noted *Give P values as exact values whenever suitable.*
☒	☐	For Bayesian analysis, information on the choice of priors and Markov chain Monte Carlo settings
☒	☐	For hierarchical and complex designs, identification of the appropriate level for tests and full reporting of outcomes
☒	☐	Estimates of effect sizes (e.g. Cohen's *d*, Pearson's *r*), indicating how they were calculated

Our web collection on statistics for biologists contains articles on many of the points above.

Software and code

Policy information about availability of computer code

Data collection	Electrical model simulations were performed using the full-custom circuit modeling and simulation software (Cadence Virtuoso IC1.6.8-64b).
Data analysis	The plots in this manuscript were generated using OriginPro (2017 Academic), and MATLAB (version R2018b). No custom data analysis was performed.

For manuscripts utilizing custom algorithms or software that are central to the research but not yet described in published literature, software must be made available to editors and reviewers. We strongly encourage code deposition in a community repository (e.g. GitHub). See the Nature Research guidelines for submitting code & software for further information.

Data

Policy information about availability of data

All manuscripts must include a data availability statement. This statement should provide the following information, where applicable:

- Accession codes, unique identifiers, or web links for publicly available datasets
- A list of figures that have associated raw data
- A description of any restrictions on data availability

The authors declare that [the/all other] data supporting the findings of this study are available within the paper [and its supplementary information files].

Field-specific reporting

Please select the one below that is the best fit for your research. If you are not sure, read the appropriate sections before making your selection.

☐ Life sciences ☐ Behavioural & social sciences ☐ Ecological, evolutionary & environmental sciences

For a reference copy of the document with all sections, see nature.com/documents/nr-reporting-summary-flat.pdf

Life sciences study design

All studies must disclose on these points even when the disclosure is negative.

Sample size	*Describe how sample size was determined, detailing any statistical methods used to predetermine sample size OR if no sample-size calculation was performed, describe how sample sizes were chosen and provide a rationale for why these sample sizes are sufficient.*
Data exclusions	*Describe any data exclusions. If no data were excluded from the analyses, state so OR if data were excluded, describe the exclusions and the rationale behind them, indicating whether exclusion criteria were pre-established.*
Replication	*Describe the measures taken to verify the reproducibility of the experimental findings. If all attempts at replication were successful, confirm this OR if there are any findings that were not replicated or cannot be reproduced, note this and describe why.*
Randomization	*Describe how samples/organisms/participants were allocated into experimental groups. If allocation was not random, describe how covariates were controlled OR if this is not relevant to your study, explain why.*
Blinding	*Describe whether the investigators were blinded to group allocation during data collection and/or analysis. If blinding was not possible, describe why OR explain why blinding was not relevant to your study.*

Behavioural & social sciences study design

All studies must disclose on these points even when the disclosure is negative.

Study description	*Briefly describe the study type including whether data are quantitative, qualitative, or mixed-methods (e.g. qualitative cross-sectional, quantitative experimental, mixed-methods case study).*
Research sample	*State the research sample (e.g. Harvard university undergraduates, villagers in rural India) and provide relevant demographic information (e.g. age, sex) and indicate whether the sample is representative. Provide a rationale for the study sample chosen. For studies involving existing datasets, please describe the dataset and source.*
Sampling strategy	*Describe the sampling procedure (e.g. random, snowball, stratified, convenience). Describe the statistical methods that were used to predetermine sample size OR if no sample-size calculation was performed, describe how sample sizes were chosen and provide a rationale for why these sample sizes are sufficient. For qualitative data, please indicate whether data saturation was considered, and what criteria were used to decide that no further sampling was needed.*
Data collection	*Provide details about the data collection procedure, including the instruments or devices used to record the data (e.g. pen and paper, computer, eye tracker, video or audio equipment) whether anyone was present besides the participant(s) and the researcher, and whether the researcher was blind to experimental condition and/or the study hypothesis during data collection.*
Timing	*Indicate the start and stop dates of data collection. If there is a gap between collection periods, state the dates for each sample cohort.*
Data exclusions	*If no data were excluded from the analyses, state so OR if data were excluded, provide the exact number of exclusions and the rationale behind them, indicating whether exclusion criteria were pre-established.*
Non-participation	*State how many participants dropped out/declined participation and the reason(s) given OR provide response rate OR state that no participants dropped out/declined participation.*
Randomization	*If participants were not allocated into experimental groups, state so OR describe how participants were allocated to groups, and if allocation was not random, describe how covariates were controlled.*

Ecological, evolutionary & environmental sciences study design

All studies must disclose on these points even when the disclosure is negative.

Study description	*Briefly describe the study. For quantitative data include treatment factors and interactions, design structure (e.g. factorial, nested, hierarchical), nature and number of experimental units and replicates.*
Research sample	*Describe the research sample (e.g. a group of tagged Passer domesticus, all Stenocereus thurberi within Organ Pipe Cactus National*

Research sample	*Monument), and provide a rationale for the sample choice. When relevant, describe the organism taxa, source, sex, age range and any manipulations. State what population the sample is meant to represent when applicable. For studies involving existing datasets, describe the data and its source.*
Sampling strategy	*Note the sampling procedure. Describe the statistical methods that were used to predetermine sample size OR if no sample-size calculation was performed, describe how sample sizes were chosen and provide a rationale for why these sample sizes are sufficient.*
Data collection	*Describe the data collection procedure, including who recorded the data and how.*
Timing and spatial scale	*Indicate the start and stop dates of data collection, noting the frequency and periodicity of sampling and providing a rationale for these choices. If there is a gap between collection periods, state the dates for each sample cohort. Specify the spatial scale from which the data are taken*
Data exclusions	*If no data were excluded from the analyses, state so OR if data were excluded, describe the exclusions and the rationale behind them, indicating whether exclusion criteria were pre-established.*
Reproducibility	*Describe the measures taken to verify the reproducibility of experimental findings. For each experiment, note whether any attempts to repeat the experiment failed OR state that all attempts to repeat the experiment were successful.*
Randomization	*Describe how samples/organisms/participants were allocated into groups. If allocation was not random, describe how covariates were controlled. If this is not relevant to your study, explain why.*
Blinding	*Describe the extent of blinding used during data acquisition and analysis. If blinding was not possible, describe why OR explain why blinding was not relevant to your study.*

Did the study involve field work? ☐ Yes ☐ No

Field work, collection and transport

Field conditions	*Describe the study conditions for field work, providing relevant parameters (e.g. temperature, rainfall).*
Location	*State the location of the sampling or experiment, providing relevant parameters (e.g. latitude and longitude, elevation, water depth).*
Access & import/export	*Describe the efforts you have made to access habitats and to collect and import/export your samples in a responsible manner and in compliance with local, national and international laws, noting any permits that were obtained (give the name of the issuing authority, the date of issue, and any identifying information).*
Disturbance	*Describe any disturbance caused by the study and how it was minimized.*

Reporting for specific materials, systems and methods

We require information from authors about some types of materials, experimental systems and methods used in many studies. Here, indicate whether each material, system or method listed is relevant to your study. If you are not sure if a list item applies to your research, read the appropriate section before selecting a response.

Materials & experimental systems

n/a	Involved in the study
☒	☐ Antibodies
☒	☐ Eukaryotic cell lines
☒	☐ Palaeontology and archaeology
☒	☐ Animals and other organisms
☐	☒ Human research participants
☒	☐ Clinical data
☒	☐ Dual use research of concern

Methods

n/a	Involved in the study
☒	☐ ChIP-seq
☒	☐ Flow cytometry
☒	☐ MRI-based neuroimaging

Human research participants

Policy information about studies involving human research participants

Population characteristics	Measurements of the body-coupling characteristics, the body-coupled power transmission and harvesting were performed with 4 healthy subjects (2 females and 2 males), aged 25 to 40.
Recruitment	Consenting subjects were recruited from within the research group from National University of Singapore as well as Masdar Institute of Science and Technology (now Khalifa University).
Ethics oversight	Human Subjects Research Ethics Committee (HSREC) of Masdar Institute of Science and Technology.

Note that full information on the approval of the study protocol must also be provided in the manuscript.